Journal of Nuclear Materials 514 (2019) 299–310

Contents lists available at ScienceDirect

Journal of Nuclear Materials

journal homepage: www.elsevier.com/locate/jnucmat

The role of chemical disorder and structural freedom in radiation-induced amorphization of silicon carbide deduced from electron spectroscopy and *ab initio* simulations

Alexander J. Leide [a, c, *], Linn W. Hobbs [a, b], Ziqiang Wang [a], Di Chen [d], Lin Shao [d], Ju Li [a, b]

[a] Department of Materials Science and Engineering, Massachusetts Institute of Technology, 77 Massachusetts Avenue, Cambridge, MA, 02139-4307, USA
[b] Department of Nuclear Science and Engineering, Massachusetts Institute of Technology, 77 Massachusetts Avenue, Cambridge, MA, 02139-4307, USA
[c] Department of Materials, University of Oxford, Parks Road, Oxford, OX1 3PH, UK
[d] Department of Nuclear Engineering, Texas A&M University, College Station, TX, 77843-3133, USA

HIGHLIGHTS

- Additional structural freedom is required for {4,4} connected networks to amorphize.
- Structural freedom in SiC is achieved by C-C bonding (chemical disorder).
- C-C homonuclear bonding allows for sp2 bond hybrids and 3-fold connected carbon.
- Local clusters and primitive rings can identify differences in aperiodic structures.
- "Amorphous" structures are identifiably different depending on how they are created.

GRAPHICAL ABSTRACT

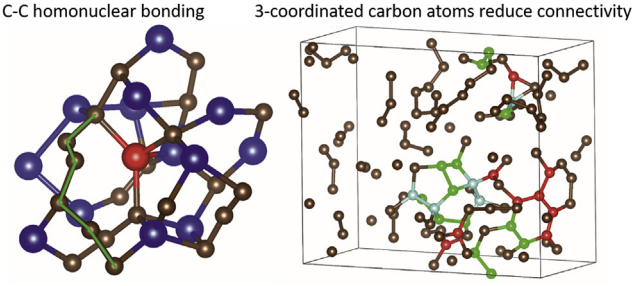

ARTICLE INFO

Article history:
Received 27 February 2018
Received in revised form
22 November 2018
Accepted 27 November 2018
Available online 28 November 2018

Keywords:
Silicon carbide
Amorphization
Radiation damage
EELS
Ab initio simulation
Disorder

ABSTRACT

Chemical disorder has previously been proposed as an explanation for the anomalously facile amorphization of silicon carbide (SiC), on the basis of topological connectivity arguments alone. In this exploratory study, "amorphous" (formally, *aperiodic*) SiC structures produced in *ab initio* molecular dynamics simulations were assessed for their connectivity topology and used to compute synthetic electron energy-loss spectra (EELS) using the *ab initio* real-space multiple scattering code FEFF. The synthesized spectra were compared to experimental EELS spectra collected from an ion-amorphized SiC specimen. A threshold level of chemical disorder χ (expressed as the ratio of the number of carbon-carbon bonds to the number of carbon-silicon bonds) was found to be $\chi \approx 0.38$, above which structural relaxation resulted in formally aperiodic structures. Different disordering methodologies resulted in identifiably different aperiodic structures, as assessed by local-cluster analysis and confirmed by collecting near-edge electron energy-loss spectra (ELNES). Such structural differences are predicted to arise for SiC crystals amorphized by irradiations involving different damage mechanisms—and therefore differing disordering mechanisms—for example, when contrasting the respective amorphized products of ion irradiation, neutron irradiation, and high-energy electron irradiation. Evidence for sp^2-hybridized carbon bonding is observed, both experimentally in the irradiated sample and in simulations, and related to connectivity topology-based models for the amorphization of silicon carbide. New information about the probable intermediate-range structures present in amorphized silicon carbide is deduced from enumeration of

* Corresponding author. Current address: Department of Materials, University of Oxford, Parks Road, Oxford, OX1 3PH, UK.
E-mail address: alexander.leide@materials.ox.ac.uk (A.J. Leide).

https://doi.org/10.1016/j.jnucmat.2018.11.036

primitive rings and evolution of local cluster configurations during the *ab initio*-modelled amorphization sequences.

1. Introduction

Silicon carbide (SiC) is a structural ceramic material useful in extreme environments because of its excellent high-temperature properties, including creep resistance, high strength, corrosion resistance and general chemical inertness, high thermal conductivity, and low thermal expansion coefficient [1–3]. More specifically, SiC is being considered for nuclear applications due to its low neutron absorption cross section, stability under high-temperature neutron irradiation at elevated temperatures, and inherently low level of long-lived radioisotopes produced through nuclear transmutations [1,3–7]. These properties make it a suitable material for structural and cladding components of fission reactors [8]; blanket components of fusion reactors [4,5,9]; encapsulation media for storing radioactive waste [10]; and components of Tri-Structural Isotropic (TRISO) and other fuel-pellet designs for advanced fission reactor concepts [11]. SiC is also a wide band-gap semiconductor that retains its semiconducting properties to high temperatures, making it useful for devices operating at high power and high frequency, and in high temperature environments (though, unfortunately, dopable only by ion implantation [12]). Somewhat surprisingly, SiC has been found to be anomalously susceptible to amorphization by atomic displacements [4–7] during irradiation below critical radiation temperatures not far above room temperature (T_c ~ 500–700 K, depending on irradiation type), resulting in macroscopic swelling, changes to mechanical properties, and electronic structure changes.

1.1. Structure, connectivity topology, local-clusters, and the amorphization anomaly

SiC crystallizes into a cubic β-SiC polymorph, with the cubic zincblende structure; a hexagonal α-SiC polymorph, with the hexagonal wurtzite structure; and a large family of hexagonal or rhombohedral α-SiC longer-period polytypes that effectively employ both structural motifs in combination. The crystalline forms do not melt but instead decompose and sublime at very high temperature (~2970 K). Both carbon and silicon atoms are each tetrahedrally-coordinated to four atoms of the opposite sort in covalent Si-C bonds and, heuristically, can be thought to form virtual [SiC_4] (or [CSi_4]) tetrahedron units that link fully by multiply sharing all vertices.

Cubic β-SiC (the 3C polymorph in the Ramsdell [13] notation) has the zincblende structure; alternatively, it can be variously described as two interpenetrating face-centred cubic sublattices of carbon and silicon atoms, or geometrically as the three-layer repeat stacking sequence … *c(abc)ab* … (hence 3C in the Ramsdell notation) of puckered hexagonal-net sheets. The α-SiC hexagonal or rhombohedral polytypes can be analogously thought of as based fundamentally on a two-layer … b*(ab)a* … stacking sequence (the 2H polymorph, with the wurtzite structure), four-layer … *cb(abcb)ab* … stacking (the 4H polytype), or six-layer … *acb(abcacb)abc* … stacking (the 6H polytype) of the same puckered hexagonal nets. Other polytypes comprise longer-period combinations of the cubic and hexagonal stacking sequences.

Connectivity in structures can be represented by {*v*,*c*}, where *v* is the number of vertices of a fundamental repeated structural unit (or *polytope*), and *c* is the number of structural polytopes connected at a polytope vertex. All these SiC structures can be considered to consist of [SiC_4] (or [CSi_4]) four-vertex tetrahedral polytopes linked four-tetrahedra-to-a-vertex, an eponymous {4,4} connectivity scheme that can result in either the cubic β-SiC structure or the hexagonal or rhombohedral α-SiC polytypes. Enumeration of atom-by-atom topological connectivities can be applied to describe their intermediate-range structures. The 2H hexagonal and 3C cubic polymorphs, representing the two fundamental assembly motifs, are topologically similar but not identical [14]: numerically identical in their primitive ring complement (12 six-atom rings); but differing slightly in their intermediate-range structures, as described by local topological clusters, Fig. 1 [15], respectively comprising the 27 atoms (2H α-SiC) or 29 atoms (3C β-SiC) that are each nodes of one of the 12 six-atom primitive rings passing through a given Si or C origin atom. (A reader unfamiliar with this connectivity-based approach to atom assemblies should consult references [14,15] for nomenclature and definitions of ring and local cluster used in connectivity topology analysis, using the formalism first introduced by Marians and Hobbs [16,17] for polytope connections and later generalized to atom-to-atom connections [15]).

The {4,4} connectivity of tetrahedra in crystalline SiC structures defines a structural freedom parameter [18] value of $f = -3$, based on the formalism introduced by Gupta and Cooper [19], where f is the difference between the degrees of freedom (3, in three-dimensional assemblies) available to a given polytope (in this case a [SiC_4] tetrahedron) and the constraints on that unit by its connections to neighboring units. A negative value signifies over-constraint, *viz* a larger number of polytope constraints than available degrees of polytope freedom. Other tetrahedral silicon-based ceramics, such as silicon nitride (α- or β-Si_3N_4) [14] and tetrahedral silica (SiO_2) polymorphs [20,21] have, respectively, three (with {4,3} connectivity) or two (with {4,2} connectivity) tetrahedra connected at each tetrahedron vertex, resulting in respective structural freedom parameters of $f = -1.5$ and $f = 0$ [18].

With no excess structural constraints ($f = 0$) in SiO_2 tetrahedral assemblies, it is easily possible to generate stable non-crystalline arrangements by disconnecting, disordering, and reconnecting tetrahedra (for example, by bond-switching or using deviant local generation rules in self-assembly modelling [14]), and experimentally evidenced [22] by the facile amorphization of tetrahedral silica polymorphs during processes of irradiation-induced atom displacement, bond severance and recovery. The significant *over*-constraint in Si_3N_4 ($f = -1.5$) renders such non-crystalline reassembly sequences unlikely, with energetically-costly bond stretches [14]; and indeed there is no evidence demonstrated for amorphizability of Si_3N_4, in either of its two crystalline polymorphic forms [14,15].

Such *non*-crystalline re-assembly sequences for the *even more* over-connected tetrahedra in SiC engender an unphysical accumulation of broken bonds and thus prove impossible to impose [14,15], suggesting that it should be very difficult or impossible to amorphize SiC if the connectivity constraints (including chemical order) are largely maintained. Hobbs and co-workers [15,18] have previously shown a surprisingly good correlation between structural freedom parameter, *f*, and ease of irradiation-induced

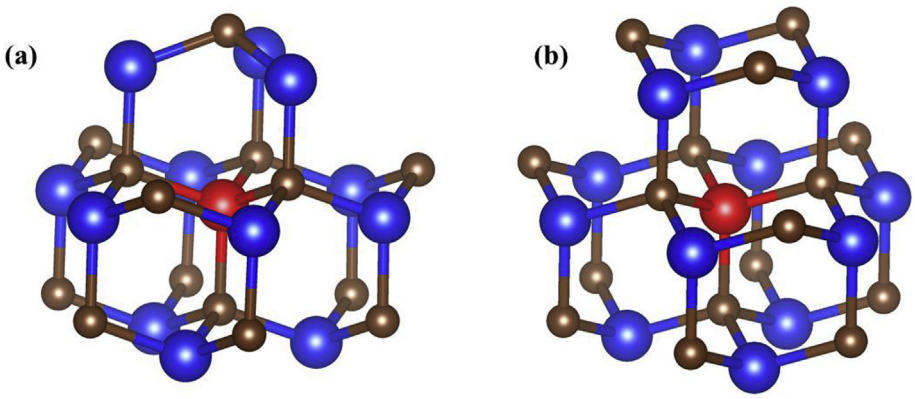

Fig. 1. Si-centred local clusters for silicon carbide crystalline polymorphs. a) Hexagonal α-SiC (2H polymorph) local cluster, comprising the 27 atoms (13 Si, 14 C) that are part of the 12 6-atom primitive rings depicted. b) Cubic β-SiC (3C polymorph) local cluster, exhibiting the same ring complement, but instead comprising 29 atoms (13 Si, 16 C). Corresponding carbon-centred local clusters would, respectively, be topologically identical to the two depictions above (with the atom colors and sizes in the depictions reversed and their atom counts reversed). (For interpretation of the references to color in this figure legend, the reader is referred to the Web version of this article.)

amorphization, assessed over a large range of inorganic structures and chemistries, and SiC is a notable outlier in that correlation. SiC is especially anomalous in that its displacive-energy dose for amorphization can be as low as ~13 eV/atom (not far from that for amorphization of SiO_2, ~7 eV/atom), suggesting a correlated structural freedom $-1 < f < 0$, instead of the expected ~100 eV/atom measured for other inorganic compounds whose crystal structures yield values around $f = -3$. Small differences in the amorphizabilities of α- and β-SiC polymorphs are also observed and likely originate in the subtle difference between their intermediate-range structures, as reflected in the small difference in local-cluster atom complements for the two polymorphs.

One explanation previously proposed for this striking anomaly is the potential for chemical disorder in SiC, a compound comprised of two group IV elements with a significant difference in covalent radii (C, 77 pm; Si, 111 pm), each of which can form isostructural elemental solids with tetrahedral bonding geometry. A completely random distribution of Si and C atoms on the SiC atom sites renders the assembly *topologically* identical to silicon (or diamond carbon) with an average atom occupancy, though of course accompanied by local structural relaxation strains in the vicinity of the Si-Si or C-C homonuclear bonds necessarily arising as an accompanying consequence.

Such a randomization in atom distribution can be initially facilitated by introduction of pairwise anti-site disorder, in which silicon atoms sit on carbon sites, and carbon atoms on silicon sites; but as the number of such isolated anti-site defects increases there is a point at which it becomes impossible to identify what is properly a Si site and what is a C site—that is, to identify complete $[SiC_4]$ or $[CSi_4]$ tetrahedra—and a simple polytopic topological description of the structure as vertex-sharing $[SiC_4]$ or $[CSi_4]$ tetrahedra fails. The loss of an identifiable $[SiC_4]$ or $[CSi_4]$ coordination tetrahedron reduces the connectivity constraints, hence introduces increased freedom for structural rearrangement [18] through various damage and recovery mechanisms during irradiation.

It is possible to depict crystalline silicon (or a fully chemically-disordered crystalline SiC comprising random occupation of atom sites by Si and C atoms, with an "average silicon" atom <Si> occupation) as an assembly of vertex-sharing virtual $[<Si> \times_4]$ tetrahedra with {4,2} connectivity, where × represents a bond-midpoint, and the <Si>– × -<Si> angle is constrained to be 180°. This description of crystalline silicon (or fully chemically-disordered crystalline SiC) is in fact isostructural with that of ideal cristobalite-SiO_2, whose structural freedom parameter is $f = 0$ and whose crystalline form is readily amorphizable (at ~7 eV/atom), but in which compound the Si-O-Si angle is *not* constrained to be 180°. The additional angular constraint introduced to ensure a linear Si-Si bond in the analogous depiction of elemental silicon [23] or a fully chemically-disordered SiC (with the <Si>– × -<Si> angle rigidly constrained to be 180°) removes some of that structural freedom available to SiO_2-cristobalite, so one expects $f < 0$ for silicon [15,18], which consequently is expected to (and does) amorphize at somewhat larger deposited energy densities (~13 eV/atom).

1.2. Prior studies of amorphous SiC

Tersoff proposed measuring the chemical disorder in SiC using a chemical disorder parameter χ, defined as the number of carbon-carbon homonuclear bonds divided by the number of carbon-silicon heteronuclear bonds [24]. Yuan and Hobbs [25] were first to demonstrate amorphization of SiC by introducing chemical disorder into a perfect crystal model and relaxing the result using molecular dynamics, finding an amorphization threshold at $\chi \approx 0.3–0.4$ and significant retention of chemical disorder after amorphization. Classical molecular dynamics (MD) simulations are limited by the interatomic potentials applied, which can significantly influence what structures form. Yuan and Hobbs [25,26] showed that adoption of different Tersoff potentials for SiC greatly influenced the structures resulting from the introduction of chemical disorder, because certain of them mediated against C-C homonuclear bond formation. Rino et al., in their classical MD study of short- and medium-range structural correlations in amorphous SiC [27], found complete retention of chemical order, while Gao et al. [6] in their classical MD modelling of radiation-induced amorphization of SiC found instead significant evidence for chemical disorder present.

Debelle et al. [28] used classical molecular dynamics simulations of collision cascade overlaps and random Frenkel pair accumulation, along with high-resolution X-ray diffraction experiments of ion-implanted amorphizing SiC to describe the process of amorphization. A crystallographic description of disorder based on Frenkel pairs in a Wigner-Seitz cell was used, because the effect of this defect distribution can ostensibly be measured experimentally as well as modelled (though, importantly, only up to the point that the notion of a crystalline reference lattice is lost;—see a demonstration of this limitation in damaged SiC in ref. [[15]). Their

experiments and modelling support the two-step process of amorphization proposed by Gao and Weber [29]: in step 1, point defects accumulate and raise the elastic energy of the system until, in step 2, a point is reached at which defect clusters relax into amorphous domains. This description of amorphization has been widely accepted; nevertheless, it does not fully describe the anomalously easy amorphization of SiC, nor does it address the inherent difficulty of identifying crystallographic point defects (or their aggregates) where long-range fixed references are significantly lost. For the latter case, only "defect" identifications based on local topological connectivity can unambiguously assess the true defect accumulation density and their state of aggregation (consult [15] for application to SiC).

An additional consequence of introducing crystallographic Frenkel pairs to a covalent crystal is homonuclear bonding, or chemical disorder. Some vacancies and interstitials will recombine into anti-sites within a crystallographic definition: $V_{Si} + C_i \rightarrow C_{Si}$ (or *vice versa*). Residual interstitial atoms will be chemically bonded to their nearest neighbours, including homonuclear bonds. Likewise, atoms around vacancies will relax in an attempt to avoid underconnection in the network introducing homonuclear bonds. Although not direct formal crystallographic anti-site pair formation, these defects introduce chemical disordering as well as structural disorder. "Crystallographic" defects are unable to exist in SiC without the introduction of "chemical" defects.

Ab initio molecular dynamics methods can be expected to more confidently depict the state of chemical disordering and of homonuclear bond formation. Finocchi [30] found 40–45% homonuclear carbon bonds, and evidence for sp^2-and sp^3-bonded carbon atoms forming chains in melt-quenches. Li [31] amorphized SiC by introducing chemical disorder into small simulation cells of perfect SiC and relaxing using *ab initio* MD. This procedure resulted in chemically-disordered amorphous SiC, which became metallic at high disorder. He proposed that lattice shear and hydrostatic strains created by chemical disordering facilitated amorphization. More recently, Jiang et al. [32] simulated electron-irradiation displacement damage using *ab initio* MD and suggested that amorphization results from structural instability of the silicon sub-lattice, which causes a collapse of the crystal structure, and asserted that chemical disorder is thus not required for amorphization.

Various experimental spectroscopy techniques have been used to study the bonding chemistry of amorphous SiC. Electron energy-loss near-edge structure (ELNES) spectroscopy [33] was used by McKenzie et al. [34] to study amorphous SiC samples made by electron-beam evaporation of crystalline SiC, and by deposition from silane and methane gases to create hydrogenated amorphous SiC. More recently Muto et al. [35–37] studied electron irradiation-amorphized silicon carbide. Hydrogenated amorphous SiC showed a significant π^* peak at 284 eV in the carbon K-edge, corresponding to a transition from 1s to a π^* anti-bonding state. This transition is indicative of graphitic sp^2-hybrid trigonal (instead of sp^3-hybrid tetrahedral) bonding of 3-connected C atoms. In contrast, the electron-irradiated specimens showed no π^* peak, thus no evidence of 3-connected C atoms. Results from other spectroscopy techniques applied to irradiated SiC are in conflict on the issue of homonuclear carbon-carbon bond formation, variously represented as evidence for everything from unaltered short-range order to complete absence of chemical ordering [38–46].

Electron diffraction [47,48] and X-ray absorption fine structure (EXAFS) measurements [49] have been used to generate radial distribution functions for ion-implantation-amorphized SiC. Based on approximate bond lengths, peaks corresponding to C-C and Si-Si homonuclear bonding were identified, in support of the presence of chemical disordering. The C-C bond length implied by the radial distribution functions deduced from electron diffraction was 1.51 Å, which is between the nearest-neighbor distances for graphite (1.43 Å), and diamond (1.55 Å). The result suggests the presence of sp^2-bonded carbon atoms, although their existence was not directly confirmed.

2. Methods

2.1. Simulation details

Two types of molecular dynamics simulations were carried out: 1) quenches from a 6000 K liquid precursor to 300 K; and 2) artificially imposed introduction of chemical disorder in a β-SiC precursor by random atom swapping at 300 K. The Vienna *ab initio* Simulation Program (VASP) [50] was used to carry out simulations, employing simulation cells comprising 216 atoms, with periodic boundary conditions imposed. The Perdew-Berke-Ernzerhof generalized gradient approximation (GGA-PBE) [51] exchange-correlation functional was used with the appropriate projector augmented-wave pseudopotential (PAW-PBE) [52]. The plane-wave expansion cut-off energy was set to 600 eV, and the Brillouin zone was sampled using a $2 \times 2 \times 2$ Monkhorst-Pack grid [53]. Electronic relaxation was allowed to proceed until the change in energy was less than 0.1 meV, while ionic and supercell relaxations were continued until the energy change was less than 1 meV. Staging of the molecular dynamics employed a Nosé-Hoover thermostat [54] in the canonical ensemble, with a 1fs timestep.

The lattice parameter of perfect 3C β-SiC crystal emerging from the *ab initio* simulation at 300 K was 0.43784 nm, 0.43% larger than the accepted experimental lattice parameter. Random atom swaps were made in this static β-SiC crystalline assembly to impose initial chemical disorder values of $\chi_0 = 0.09$, 0.17, 0.22, 0.27, 0.29, 0.31, 0.35, 0.38, 0.42, 0.46, 0.5, 0.53, and 0.58, with the adopted chemical disorder parameter defined [24] as χ = (number of C-C homonuclear bonds) divided by (number of C-Si heteronuclear bonds). The disordered assemblies were then relaxed by MD at 300 K for 3 ps, followed by conjugate-gradient supercell relaxation.

For simulation of structures formed by quenching from the liquid state, the relaxed 3C β-SiC crystalline assembly was melted for 2 ps at 6000 K, at which temperature diffusive motion of atoms was observed. A time step of 1 fs was used, and after every 400 fs of MD the simulation cell was relaxed using the conjugate-gradient algorithm. Partial radial distribution functions showed no meaningful ordering beyond first neighbours, as expected for a liquid. The quenching rate imposed was 9.83×10^{14} K/s, significantly faster than experimentally obtainable quenches, even in ballistic collision cascades where it is of order 10^{11} K/s. The quenched assemblies were subsequently relaxed by MD at 300 K for 3 ps, followed by conjugate-gradient supercell relaxation.

A Green's function-based *ab initio* real-space multiple scattering code FEFF9, version 9.6.4 [55] was used to simulate electron energy-loss near-edge structure (ELNES) spectra [33], as implemented by Rehr and co-workers [56–58]. The multiple-scattering and self-consistent field radii were set to 0.4 nm and 0.3 nm respectively. The exchange-correlation energy was represented by the Hedin-Lundqvist self-energy, and core holes by a random-phase approximation (RPA) parameterization of the Bethe-Salpeter equations.

2.2. Experimental details

A single-crystal 6H-SiC wafer sample with dimensions $10 \times 10 \times 0.3$ mm thick, obtained by one of us (DC) from the Ion Beam Group at Texas A&M University, was irradiated with 1.35 MeV Fe^+ ions at a flux of 6.8×10^{15} ions/m^2/s to a total fluence of approximately 1×10^{20} ions/m^2. The crystal was oriented with its

wafer face nearly normal to the direction of the ion beam, which during beam scanning made an angle varying between 5° and 8° with the <0001> crystal axis. Irradiation was carried out at 500 ± 2 °C. The temperature was controlled using a thermocouple and a copper heating stage behind the sample. The irradiated crystal was milled into a cross-section specimen for transmission electron microscopy (TEM) using the focussed ion-beam lift-out technique, with the original ion-entry surface protected by an evaporated Pt overlayer. The resulting TEM sample thickness was approximately 50 nm. The depth of the ion implanted layer was predicted by SRIM Monte-Carlo simulations, and the amorphous layer was identified by the characteristic "salt and pepper" speckle contrast within this region. Electron energy-loss spectra were obtained from the amorphized zone using a Gatan GIF 2001 imaging filter interfaced with a JEOL JEM-2010F field emission analytical TEM operating at 200 kV.

2.3. Structural analysis

Evaluating aperiodic structures within the framework of traditional crystallographic approaches (symmetry operations, a unit cell defining periodic translations, and a reference lattice) is clearly nonsensical, so a characteristic topological-connectivity entity equivalent to a unit cell and of similar size was selected for evaluation instead: *viz* the local topological cluster, as originally defined by Marians & Hobbs [16,17] but generalized [15,25] to atom-to-atom connections, evaluated at each atom position. The local cluster comprises all irreducible closed-circuit paths passing through an individual element of the network (*i.e.* rings without "shortcuts," defined as *primitive* rings), together with the atoms that are nodes along these primitive rings. The local clusters thus embody the local topological *connectivities* at each point in the structure (whether periodic or aperiodic), rather than the symmetries and periodicities inherent in the unit cell representation of a crystalline arrangement. The (very similar) local clusters of crystalline α- and β-SiC are shown in Fig. 1. Primitive rings and local clusters have been used previously to characterize crystalline and amorphous polymorphic forms of SiC [14,15,25], as well as polymorphic structures of crystalline and amorphous SiO_2 [15,20,21] and more complex amorphizable ceramic structures, such as zircon ($ZrSiO_4$) [15,59] and zirconolite ($CaZrSi_2O_7$) [60].

3. Simulation results

3.1. Chemical disorder

When the chemically disordered structures were relaxed, their chemical disorder parameter values invariably reduced (Table 1). Assessment of whether a structure had amorphized or not was based on compilation of radial distribution functions, visual inspection—looking for evidence of crystalline features such as periodicity and structural unit alignments (Fig. 2),—and analysis of local cluster complements (§3.5). A threshold value for initially introduced chemical disorder sufficient to induce amorphization after relaxation was found to be about $\chi_0 = 0.38$ (with post-relaxation disorder of $\chi = 0.29$).

Total radial distribution functions (rdf) for amorphous SiC assemblies adjudged amorphous show peaks around 1.5 Å and 2.5 Å, corresponding to C-C and Si-Si homonuclear bonding (Fig. 2 (e)). The quenched and $\chi_0 = 0.38$ amorphized structures exhibit lower radii for the C-C bond distance than does the non-amorphous $\chi_0 = 0.29$ structure, in close agreement with the experimentally-obtained radial distribution functions derived from the electron diffraction data of Ishimaru et al. [47,48] The difference in peak height between simulated and experimental radial distributions is attributed to the smaller atomic scattering factor of C (compared to that of Si) reducing the intensity of the C-C correlation diffraction ring in the electron diffraction pattern from which the radial distribution function was derived.

3.2. Structural changes

When atomic bonds were drawn onto the modelled assemblies, with cut-off distances based on the first minimum of the relevant *partial* radial distribution functions, 3-coordinated carbon atoms (highlighted in Fig. 3) were apparent in the amorphous SiC assemblies obtained after both melt-quenching and chemical disordering followed by subsequent relaxation, Fig. 3. Isolated 3-coordinated C atoms and chains of 3-coordinated C atoms were observed to form in the melt-quenched structures (Fig. 3a). By contrast, highly connected carbon-carbon bond networks tended to form in the amorphous assemblies resulting from deliberate chemical disordering (Fig. 3b). Occasional carbon atoms tetrahedrally coordinated to only other carbon atoms are observed in this network, as well as (more frequently) carbon atoms 3-coordinated to other C atoms in planar configurations, and C atoms tetrahedrally bonded to three C atoms and one Si atom.

In both chemically-disordered and melt-quenched amorphous structures, silicon atoms were correspondingly observed to form highly-connected tetrahedral networks dominated by Si-Si homonuclear bonding (Fig. 4).

3.3. Local clusters

Fig. 5 shows a local cluster for a selected silicon atom in a chemically-disordered amorphized assembly ($\chi_0 = 0.38$, $\chi = 0.29$).

Table 1
Assessed chemical disorder parameters before and after relaxation.

Initial chemical disorder (χ_0)	Chemical disorder after relaxing (χ)	% Decrease from initial value of χ_0	Amorphous?
0.09	0.09	0	No
0.17	0.17	0	No
0.22	0.21	4.5%	No
0.27	0.21	22%	No
0.29	0.24	17%	No
0.31	0.25	19%	No
0.35	0.30	14%	No
0.38	0.29	24%	Yes
0.42	0.33	21%	Yes
0.46	0.38	17%	Yes
0.5	0.35	30%	Yes
0.53	0.44	17%	Yes
0.58	0.43	26%	Yes
Quench	0.24	N/A	Yes

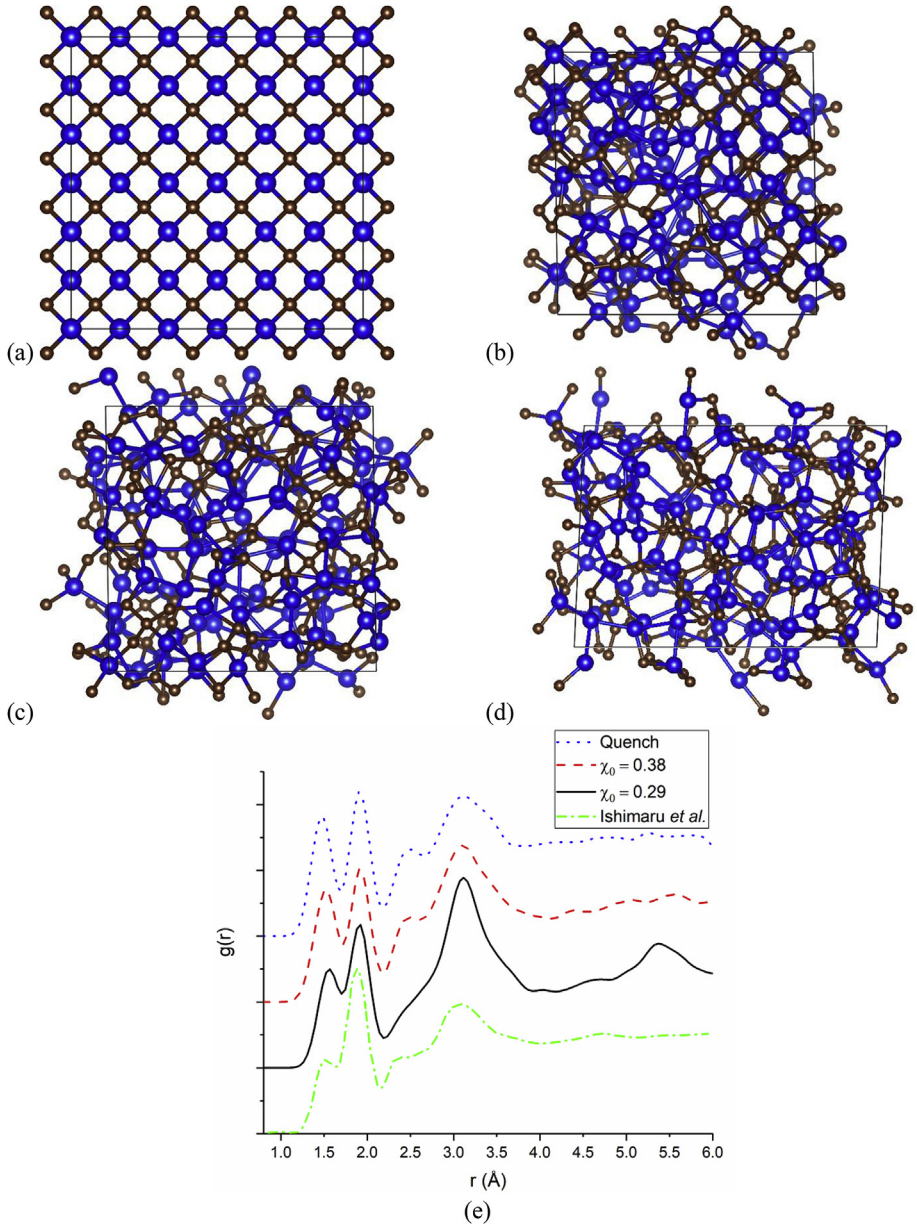

Fig. 2. SiC assemblies viewed along (100). a) Perfect crystal, b) imposed chemical disorder $\chi_0 = 0.29$ ($\chi = 0.24$), c) imposed chemical disorder $\chi_0 = 0.38$ ($\chi = 0.29$), and d) quenched ($\chi = 0.24$). Assemblies (c) and (d) were assessed to have amorphized, with few or no remanent crystalline features, while (b) was assessed to have still retained some crystalline features, visible most clearly in the upper right of the assembly. The (total) radial distribution functions for the disordered structures, together with those derived experimentally from electron diffraction patterns of Ishimaru et al. [47] (uncorrected for the different atomic scattering factors of Si and C) are shown in (e). Assembly (b) retains a peak around 5.5 Å present in the initially perfect crystal, while this peak has all but disappeared in assemblies (c) and (d).

A chain of 3-coordinated carbon atoms is highlighted, contributing to a 9-member ring. The lower coordination of carbon atoms results in lowered connectivity within the overall structure, resulting in the observed increase in average ring size in local clusters, and a similar increase in number of atoms included in local clusters, as revealed in the ring size distribution chart, Fig. 6, and the local cluster complement chart, Fig. 7.

Homonuclear carbon-carbon bonding appears to facilitate the 3-coordination of C atoms (or *vice versa*) and reduces connectivity; the carbon atoms in the carbon chains apparent in Figs. 3a and 5 comprise constituent sequential nodes in primitive rings. An observed *decrease* in overall density can in *some* circumstances be attributable to increased ring size, though larger ring sizes generally facilitate denser packing, as is observed in silicas [15,20,21]. Concurrent changes in coordination and ring size have, in any event, a synergistic and unpredictable effect on density, as demonstrated in amorphous SiO_2 or GeO_2 assemblies under pressure [61], where 4- and 6-fold Si coordination can co-exist. In the disordered SiC modelled here, the higher (and mostly retained) 4-coordination of silicon atoms serves to truncate carbon chains and to provide more frequent short-cuts that maintain smaller primitive rings. Silicon-centred local clusters contain on average more atoms than their carbon-centred counterparts (Fig. 7), due to the increasing probability that a central Si atom maintains a higher coordination than C, thus enabling more primitive rings to emanate from it.

Non 6-rings in local clusters are indicative of defects in the structure of crystalline SiC [15]. Fig. 8 displays the distribution of

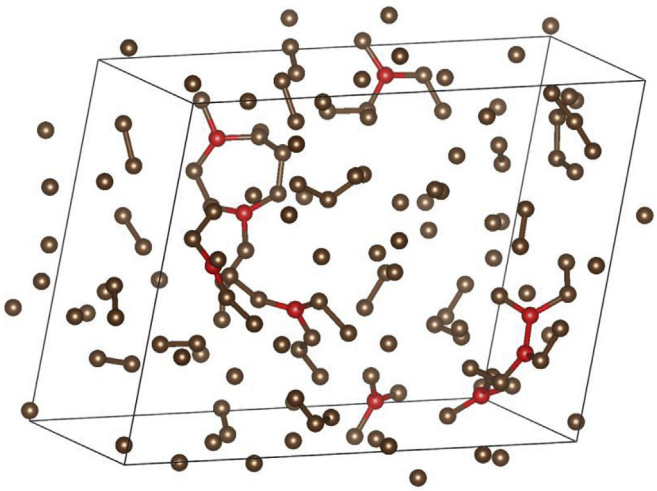

(a)

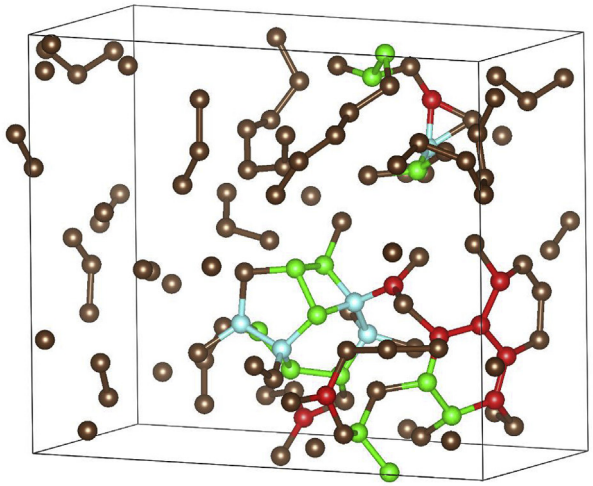

(b)

Fig. 3. Amorphous SiC assemblies resulting from (a) melt-quenching ($\chi = 0.29$), and (b) chemical disordering followed by relaxation ($\chi_0 = 0.58$, $\chi = 0.43$). Only C atoms and C-C homonuclear bonds are depicted here in both assemblies. Atoms highlighted in red are co-planar three-coordinated C; atoms highlighted in pale blue are tetrahedrally-coordinated C, connected to the network by four C-C bonds; atoms highlighted in green are tetrahedrally-coordinated C, connected to the network by three C-C bonds and one Si-C bond. (For interpretation of the references to color in this figure legend, the reader is referred to the Web version of this article.)

ring sizes in local clusters. At small amounts of imposed chemical disorder, almost all rings contain six-atom nodes (6-rings), with the number of 6-rings reducing in proportion as more chemical disorder in imposed; larger rings appear, and the ring-size distribution broadens. These developments imply significant differences in connectivity and parallel the behavior observed for other amorphizing systems. Averaged local clusters in the quenched amorphous assembly exhibit a plurality of 7-rings, while local clusters in assemblies deliberately chemically disordered still retain a plurality of 6-rings. The quenched and various imposed-disorder amorphized structures are therefore identifiably different, even though they may exhibit similar degrees of chemical disorder after relaxation (*e.g.* compare in Fig. 8 the ring-size distribution for the relaxed quenched assembly with $\chi = 0.24$ to that of the $\chi_0 = 0.29$ imposed-disorder assembly which relaxes to an identical disorder

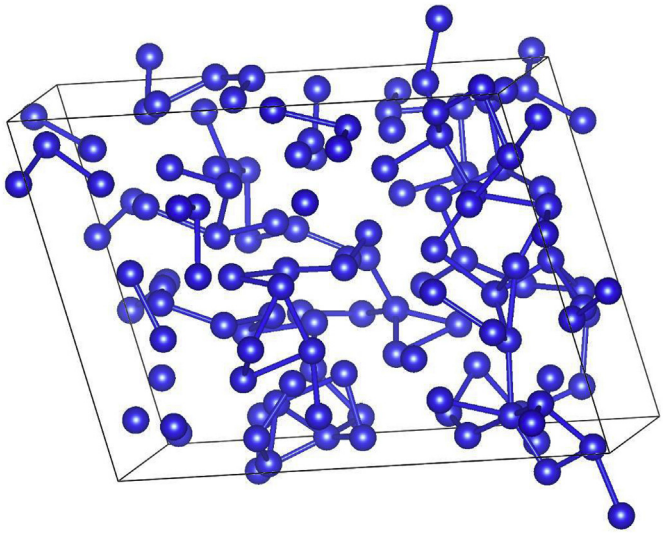

Fig. 4. Melt-quenched SiC assembly ($\chi = 0.29$), shown with only Si atoms depicted and Si-Si homonuclear bonds highlighted, reveals a substantial network of interconnected Si atoms and the beginning of an extended tetrahedral silicon network. (For interpretation of the references to color in this figure legend, the reader is referred to the Web version of this article.)

value of $\chi = 0.24$, but with a markedly different ring-size distribution), a confirmation of the consistent finding that the structures of amorphous solids depend significantly on their modes of formation.

4. Experimental and simulated ELNES data

Fig. 9 presents carbon K-edge electron energy-loss near-edge structure (ELNES) spectra, experimentally collected from unirradiated and ion-amorphized regions of a 6H α-SiC crystal specimen, and for comparison spectra simulated by the FEFF9 code, from an *ab initio* MD-generated pristine assembly of crystalline 3C β-SiC and its amorphized versions derived by quenching from a 6000 K liquid or deliberate imposition of chemical disorder. The peak at 290 eV, common to all spectra presented, is the σ* peak corresponding to sp^3 hybridized bonding. For the ion-amorphized experimental specimen, a clear additional peak is distinguishable, at 284 eV, which is similarly present in the *ab initio* MD-modelled amorphous assemblies created both by quenching and by deliberately imposed chemical disorder. This secondary peak is ascribed to the π-π* electronic transition occurring in sp^2 bonded carbon containing π bonds, for example graphitic forms of carbon. Such π bonds are unable to form between Si and C atoms in undefected SiC structures, because the tetrahedral Si-C bonding is restricted to sp^3 hybridization. Thus the presence of the 284 eV peak is suggested as direct evidence for the presence of C-C sp^2 bonding that results from 2- or 3-coordinated C network structures. The observed σ* and π* peaks both occur at lower energies compared to their positions in diamond and graphitic forms of carbon. This discrepancy may be attributable to a chemical shift of 1–2 eV due to, for example, differing bond lengths and the differing constraints in the overall environment of a SiC host. These factors can also contribute to peak broadening. Variations between simulated and experimental spectra beyond around 300 eV may be attributed to the onset of the additional electron energy-loss fine structure (EXELFS) in this spectral region that is not calculated for the simulations, because it attributable to other than electronic bonding structures. The differences in the peak *shape* below 290 eV between simulated 3C and experimental 6H crystalline SiC are artefacts of the

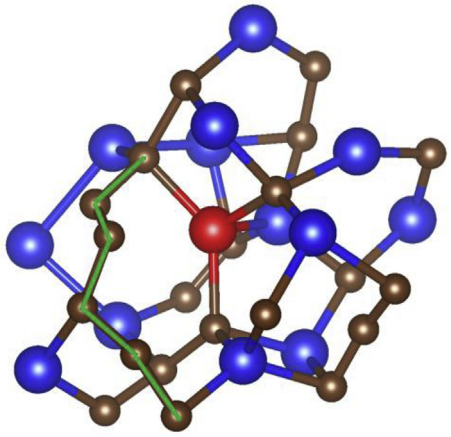

Fig. 5. Silicon local cluster from a SiC assembly with imposed chemical disorder $\chi_0 = 0.38$ ($\chi = 0.29$), showing chain of carbon atoms (highlighted in green). Si atoms are larger blue circles, C atoms smaller brown circles. Central Si atom is depicted in red. (For interpretation of the references to color in this figure legend, the reader is referred to the Web version of this article.)

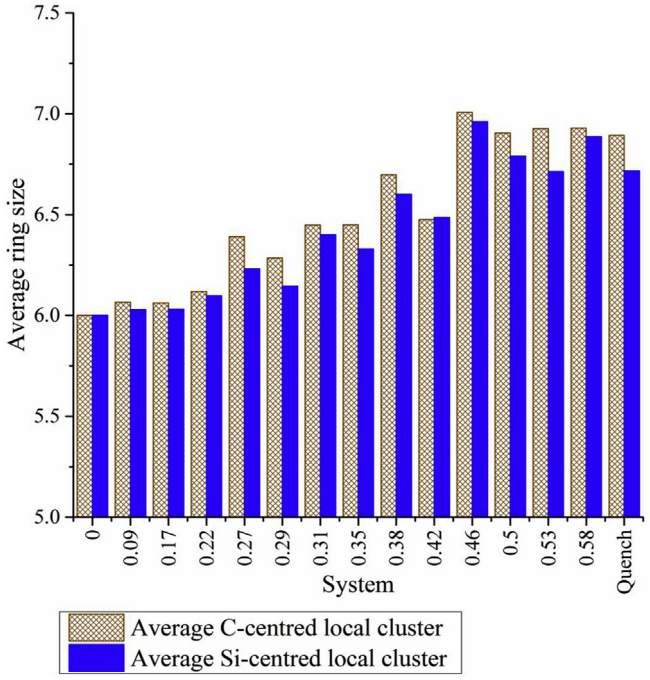

Fig. 6. Average local cluster ring sizes in various simulated disordered structures. The initial χ_0 values for imposed chemical disorder are indicated. The corresponding relaxed chemical-disorder values for these and the quenched assembly are listed in Table 1.

simulation. The steeper gradient at 292 eV in the simulated crystal is attributable to the difference between 3C and 6H SiC structures, though we should add that the *very* close similarity of the local clusters of 3C and 6H polymorphic forms (Fig. 1) nevertheless suggests that the reported comparison of spectra deduced from simulated amorphization of 3C and experimental spectra collected from amorphized 6H polymorphs remains a substantially valid exercise. Additionally, although the TEM sample was thin, the experiment is sampling a much larger volume than those represented by the small *ab initio* assemblies responsible for the simulated spectra, so longer-range energy absorption mechanisms (*e.g.* collective excitations) may be contributing to smaller minor

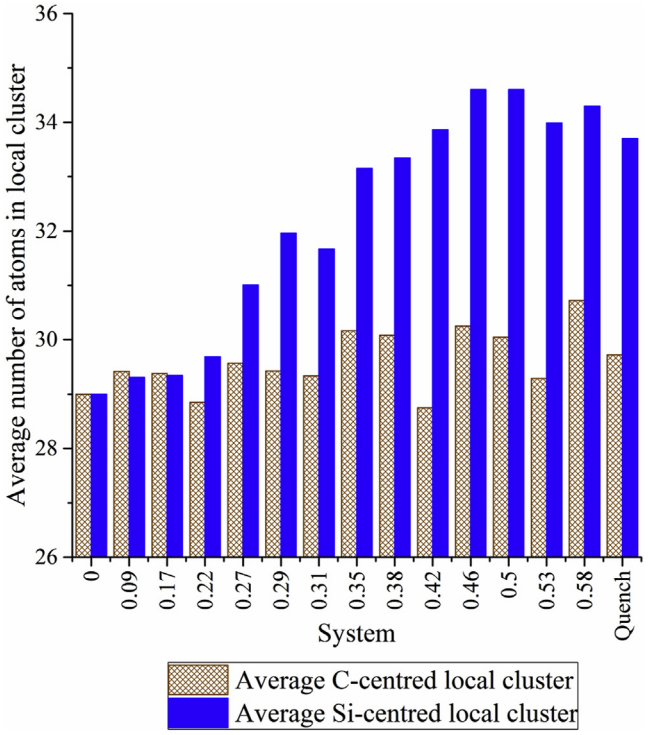

Fig. 7. Average number of atoms in local clusters for various simulated disordered structures. The initial χ_0 values for imposed chemical disorder are indicated; the corresponding relaxed chemical disorder χ values for these and the quenched assembly are listed in Table 1.

observed differences between simulated and experimental spectra.

The comparative weakness and breadth of the 284 eV peak in the simulated spectrum from the $\chi_0 = 0.53$ ($\chi = 0.44$) chemically-disordered modelled assembly, compared to the analogous peak for the simulated melt-quenched assembly, would indicate that, while there is likely some sp^2 C-C bonding present in the chemically-disordered simulation structure, the proportion is lower than that found in the melt-quenched amorphous structure, again suggesting dissimilar amorphous structures. This result is in agreement with the conclusions of the connectivity-based structural analysis.

5. Discussion

The *ab initio* modelling presented here demonstrates the importance of structural freedom in the amorphization process and suggests its necessity for an amorphization process to proceed. Based on the results of all structural analysis criteria applied, there appears to be a threshold for amorphization at an initially imposed chemical disorder about $\chi_0 = 0.38$, above which chemical disorder alone can allow sufficient structural freedom to amorphize silicon carbide, in agreement with previous model.

There is a significant difference in relaxed chemical disorder between the quenched and the chemically-disordered model structures, implying different ultimate amorphized structures accompanying the two different mechanisms of amorphization. This conclusion is supported by further structural analysis based on local clusters. Tersoff [24] suggests that graphitization may be a result dependent on the kinetics of quenching, because carbon segregation is possible in the melt. Graphitization is apparent in the simulations and could be attributed to kinetic factors because of the short timescales; however, the presence of the π^* peak in the

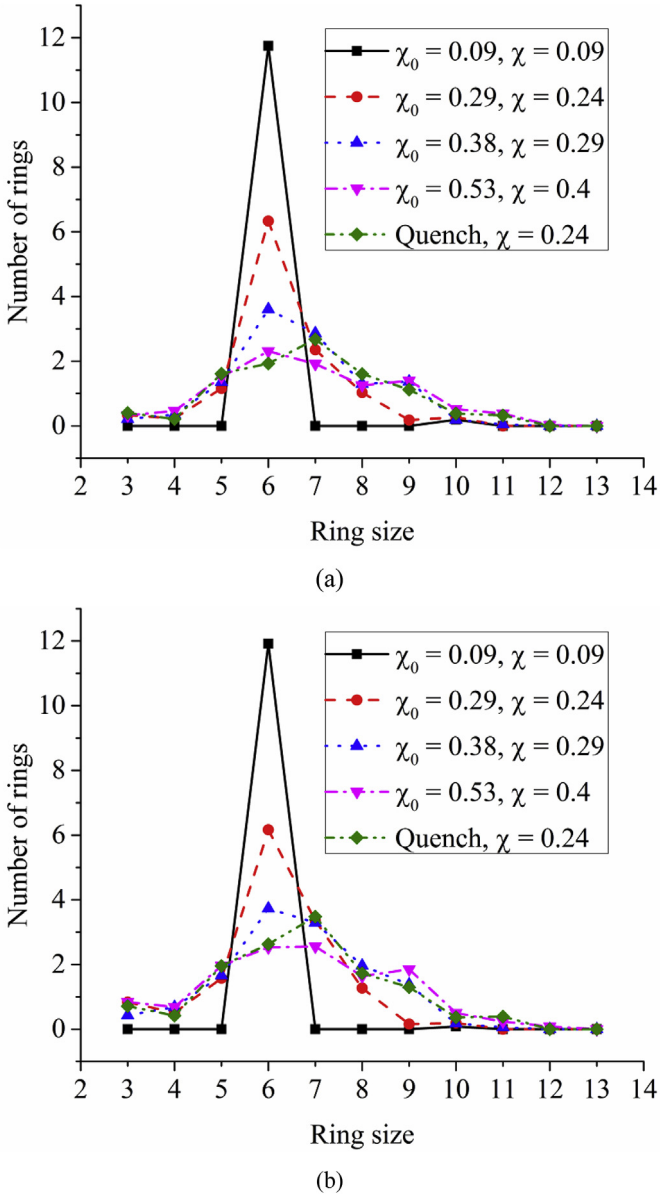

Fig. 8. Average number of rings in a) C-centred and b) Si-centred local clusters for selected simulated SiC disordered assemblies.

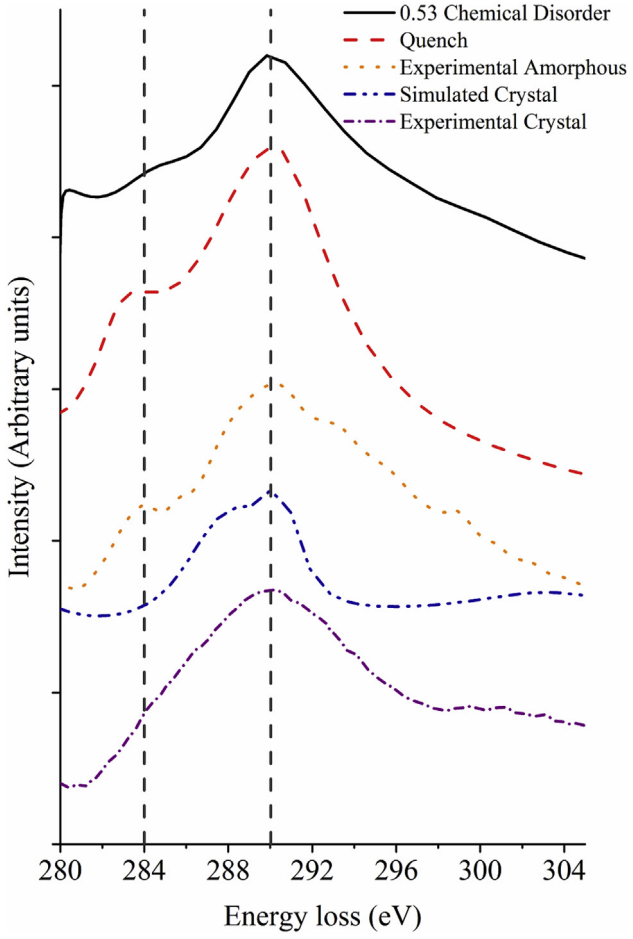

Fig. 9. Comparison of experimental carbon K-edge electron energy-loss near-edge structure (ELNES) spectra obtained from unirradiated and ion-amorphized 6H α-SiC with FEFF-simulated carbon K-edge ELNES spectra derived instead from *ab initio* MD-modelled crystalline 3C β-SiC and two SiC modelled assemblies amorphized by quenching from a liquid state at 6000 K and by deliberate imposition of chemical disorder $\chi_0 = 0.53$ ($\chi = 0.44$) in a 3C β-SiC precursor.

experimental ion-amorphized specimen cannot be attributed purely to kinetic factors in the same way. Presuming a melt-quench model of heterogeneous amorphization within a collision cascade, the quenching rate in a cooling cascade is orders of magnitude slower than the one simulated yet results in a carbon K-edge ELNES spectrum similar to that derived from the simulation. The stability of this structure over the ensuing recovery period implies that it is a rather *stable* amorphous structure, and that the observed sp^2 bonding is not purely an inherited artefact of earlier kinetic history.

The presence of a π^* peak in the experimental ion-amorphized specimen is evidence of graphitic sp^2 bonding between carbon atoms. It has been demonstrated that direct C-C homonuclear bonding exists in amorphized SiC, at least based on the results of other electron energy-loss fine structure (EXELFS) measurements from which a pseudo-radial distribution function may be extracted [35,36,62] and results of Raman scattering measurements [41–44]. However, there had previously been no direct evidence for specifically graphitic bonding. Muto et al. [35,36] observed a π^* carbon K-edge ELNES peak that disappeared during further electron irradiation while collecting ELNES spectra. They attributed its appearance to a graphite layer forming on the surface, which subsequently evaporated in the electron beam. Their observations led them to conclude that only tetrahedral sp^3 bonded carbon-carbon is present in amorphous silicon carbide. Their samples were amorphized using 1 MeV electrons in thin foils, which represent a fundamentally different damage process to that of the ion irradiation in comparative bulk used in this work. The different amorphization processes (single-atom displacements, with added potential for enhanced radiolytic contributions, in the case of electron irradiation *vs.* collision cascades in heavy ion irradiations) may explain the differences in their and our observed spectra and the probable differences in amorphous structures inferred from these spectral differences. It is worth noting that neutron irradiation-induced amorphized structures, arising in the context of fusion and fission reactor applications for SiC, should be closer to those resulting from our ion irradiation-induced amorphization than to those resulting from electron irradiation-induced amorphization involving serial single-atom displacements.

Agreement between the ELNES spectra from the ion-amorphized SiC and the melt-quench simulation suggests that

their structures could be similar. The 3-coordinated C atoms, with their co-planar bond angles separated by approximately 120° (highlighted in red in Fig. 3b) are a consequence expected from sp^2 bond hybridization, as found in graphite. This hybridization is the origin of the π^* peak observed for both experimental spectra and simulated spectra from amorphized models. Its co-appearance with the carbon chains observed in our amorphized model structures agrees with the melt-quench simulations of Finocchi [63,64], who interpreted the C chains as arising from sp^2 C-C bonding, based on structural geometry alone. Agreement between the experimentally derived and simulated ELNES spectra suggests that some features of melt-quenched and ion irradiation-amorphized structures are shared. However, the overall structures are not necessarily identical, and there is at present little direct information about intermediate-range structure collectable experimentally. The discrepancy between the present results and those reported from electron irradiation-induced amorphization experiments begs further questions relating to the probable structural differences in amorphized forms arising from different amorphization processes.

Those C atoms adopting sp^2 bond hybridization and 3-coordination contribute fewer structural constraints to a structure, thus facilitating rearrangement into aperiodic arrangements. The formation of sp^2-hybridized carbon bonds necessitates homonuclear C-C configurations in SiC, and chemical disorder is one inescapable consequence of this bonding change—one which was earlier proposed [25] as an explanation for the anomalous ease of SiC amorphization. The presence of significant homonuclear bond fractions in all modelled amorphous silicon carbide structures, whether achieved in this work or those of others, suggests that they are a necessary (and even perhaps also sufficient) requirement for SiC amorphization, in keeping with the demonstrated geometrical inability to structurally disorder silicon carbide models in the absence of homonuclear bonding, without creating severely under-connected structures [14]. Indeed, the presence of sp^2-bonded C atoms alters the connectivity by allowing under-connection relative to perfect [SiC_4] tetrahedra. Maintenance of tetrahedral sp^3-bonded C atoms would require that connectivity be maintained, but only with unacceptably large internal strains from unrealistically extended bond lengths or rotated bond angles. These arguments suggest that chemical disorder renders amorphization possible through alteration of the chemistry of C atoms in close proximity with neighboring C atoms, resulting in lowered coordinations and reduced connectivity.

Reduction in connectivity is one vital step in forming amorphous SiC structures. Jiang et al. [32] suggest that C-C homonuclear bonding is not necessary for amorphization of SiC, based on simulations where half the carbon atoms are removed from a SiC supercell (carbon vacancies, but no anti-sites are introduced), followed by *ab-initio* MD relaxation. This is an alternative—albeit unphysical (as overall stoichiometry is not maintained)—way of introducing under-connection to SiC crystalline structures, providing sufficient structural freedom for rearrangement into an aperiodic state, supporting the thesis that reduction in connectivity is vital to amorphization of SiC. Certainly, chemical disorder enables sufficient structural freedom by allowing sp^2 hybridized homonuclear C-C bonds to form while maintaining stoichiometry. The threshold level of chemical disorder could alternatively be considered as a threshold level of additional degrees of freedom enabled by formation of 3-coordinated carbon atoms. This mechanism of increasing overall structural freedom during irradiation may explain the anomalously easy amorphization of SiC relative to other tetrahedral ceramics which are unable to change their bonding hybridization. The low formation energy of anti-sites in SiC allows for sufficient homonuclear bonding, with an allowable bond length similar to that of graphitic carbon to enable anomalously easy amorphization via reduction in coordination, relative to other carbon-containing ceramics, such as ZrC, which presents a higher barrier to anti-site formation, and exhibits longer bond-lengths in the crystal, which in turn is energetically unfavorable to sp^2 C-C bond formation [32].

A second, and no less important, requirement is *stochasticity*. The displacive and chemical disordering sequences involved in amorphization can be reversed if there are simple low-energy pathways to reconstructing structures originally there and strong driving forces arising from deep crystalline wells in the structural energy landscape. Impediments to reconstruction are crucial to promotion of persisting amorphous transformations. In aperiodic silicas [15,65], local polymorphic rearrangements involving alteration of primitive ring structures provide the requisite impediment to prevent re-establishment of crystalline precursors, just as they do for transformations between crystalline silica polymorphs (such as between quartz and cristobalite). Other modelling of amorphization in more complex ceramic structures, such as zircon ($ZrSiO_4$) [15,59] has shown that segregation of chemical species during irradiation can lead to a sort of *incipient* decomposition—in the case of zircon, very localized phase separation into ZrO_2 and SiO_2 structural motifs—that does not proceed very far (only on the scale of a unit cell or, topologically, of a local cluster) but is sufficient, and sufficiently irreversible, that the disorder induced by irradiative (or other) perturbations cannot be reversed without wholesale recrystallization at very high temperature. The two key observations in irradiated or quenched SiC of 1) C-C-C strings and even formation of partial graphitic networks, and 2) [$SiSi_4$] tetrahedron formation and the beginnings of a tetrahedral silicon network, each represent the same sort of incipient decomposition that provides sufficiently strong impediment to reorganization into the original structure, and a sufficiently stochastic progression that cannot be operated in reverse, ensuring maintenance of stable aperiodic structures once formed at low homologous temperature.

Significant additional bond breakage and sufficient local diffusion of Si and C atoms are required to overcome such impediments to dynamic recrystallization, and both appear to occur in SiC only if irradiated at temperatures in excess of 700 K.

6. Conclusions

The modelling and experimental work reported here show that amorphization in silicon carbide occurs through a mechanism involving bonding changes in carbon atoms and incipient local structural segregation of both Si and C atoms, that are only made possible in the presence of *initial* chemical disorder, whether imposed by single atomic displacements (Frenkel pair production), a collision cascade, melt-quenching, or artificial atom-swapping. The ability to reduce C coordination lowers connectivity and explains the anomalous ease of silicon carbide amorphization compared to expectations based solely on the constraints imposed by its structural connectivity. This conclusion is arrived at only through the use of *ab initio* molecular dynamics modelling, where coordination number and bonding type changes are more accurately described than possible using empirical interatomic potentials in classical molecular dynamics. Thus, a more confident basis for understanding the structures of amorphous silicon carbide, and the chemical and topological progressions responsible for them, has been achieved.

Structural differences emerging from different amorphization routes, identifiable through topological connectivity analysis, have implications for the use of ion-beam or electron irradiations to model neutron irradiation damage in silicon carbides destined for nuclear applications. A deeper understanding of damage processes and their effects on resultant structures is required before relying

on any single irradiation type to provide relevant insights. The present investigation further discredits a prevalent misconception that the amorphous state is some unique entity, rather than presenting a range of polymorphic structural possibilities that are sensitive to the mode of amorphization. Distinguishable and characterizable aperiodic structures are revealed only when appropriate yardsticks are applied to elucidate intermediate-range topology.

Acknowledgments

The research described was part of the Oxford University-MIT academic exchange, with funding provided by the Worshipful Company of Armourers and Brasiers, London, and the Department of Materials, University of Oxford that made possible the seven-month stay of the corresponding author (AL) at MIT, and for which all the authors are grateful. JL acknowledges support from the US DOE Office of Nuclear Energy under Grant No. DE-NE0008827. The authors thank Dr. Lance Snead and Prof. Izabela Szlufarska for useful discussions.

References

[1] G. Newsome, L.L. Snead, T. Hinoki, Y. Katoh, D. Peters, Evaluation of neutron irradiated silicon carbide and silicon carbide composites, J. Nucl. Mater. 371 (1–3) (2007) 76–89.
[2] C.F. Zhe, Silicon Carbide: Materials, Processing & Devices, CRC Press, Boca Raton, FL, 2003.
[3] L.L. Snead, Y. Katoh, Current status and critical issues for development of SiC composites for fusion applications, J. Nucl. Mater. 371 (1–3) (2007) 659–671.
[4] Y. Katoh, L.L. Snead, I. Szlufarska, W.J. Weber, Radiation effects in SiC for nuclear structural applications, Curr. Opin. Solid State Mater. Sci. 16 (3) (2012) 143–152.
[5] M.E. Sawan, L.L. Snead, S.J. Zinkle, Radiation damage parameters for SiC/SiC composite structure in fusion nuclear environment, Fusion Sci. Technol. 44 (1) (2003) 150–154.
[6] F. Gao, W.J. Weber, W. Jiang, Primary damage states produced by Si and Au recoils in SiC: a molecular dynamics and experimental investigation, *Phys. Rev.* B 63 (21) (2001), 214106-(1-6).
[7] L.L. Snead, S.J. Zinkle, J.C. Hay, M.C. Osborne, Amorphization of SiC under ion and neutron irradiation, Nucl. Instrum. Methods Phys. Res. B 141 (1–4) (1998) 123–132.
[8] Y. Sukjai, E. Pilat, K. Shirvan, M. Kazimi, Silicon Carbide Performance as Cladding for Uranium and Thorium Fuels for Light Water Reactors," Advanced Nuclear Power Report Series, MIT-anp-tr-149, MIT, Cambridge, MA, 2014.
[9] E.T. Cheng, J.K. Garner, M. Simnad, J. Talbot, A low-activation fusion blanket with SiC structure and Pb-Li breeder, in: 15th IEEE/NPSS Symposium on Fusion Engineering vol. 1, 1993, pp. 277–281, 1993.
[10] J. Knorr, W. Lippmann, A.-M. Reinecke, R. Wolf, A. Kerber, A. Wolter, SiC encapsulation of (V)HTR components and waste by laser beam joining of ceramics, Nucl. Eng. Des. 238 (11) (2008) 3129–3135.
[11] P. Hosemann, J.N. Martos, D. Frazer, G. Vasudevamurthy, T.S. Byun, J.D. Hunn, B.C. Jolly, K. Terrani, M. Okuniewski, Mechanical characteristics of SiC coating layer in TRISO fuel particles, J. Nucl. Mater. 442 (1–3) (2013) 133–142.
[12] W. Wesch, A. Heft, E. Wendler, T. Bachmann, E. Glaser, High temperature ion implantation of silicon carbide, Nucl. Instrum. Methods Phys. Res. B 96 (1–2) (1995) 335–338.
[13] L.S. Ramsdell, Studies on silicon carbide, Am. Mineral. 32 (1–2) (1947) 64–82.
[14] C.E. Jesurum, V. Pulim, L.W. Hobbs, Topological modeling of amorphized tetrahedral ceramic network structures, J. Nucl. Mater. 253 (1–3) (1998) 87–103.
[15] L.W. Hobbs, Topological approaches to the structure of crystalline and amorphous atom assemblies, in: J.J. Novoa, D. Braga, L. Addadi (Eds.), Engineering of Crystalline Materials Properties, Springer, Cham, Switzerland, 2008, pp. 193–230.
[16] C. S Marians, L.W. Hobbs, A language for the study of network silica glasses, Diffusion Defect Data 53–54 (1988) 31–36.
[17] C.S. Marians, L.W. Hobbs, Local structure of silica glasses, J. Non-Cryst. Solids 119 (3) (1990) 269–282. L. W. Hobbs, "Network topology in aperiodic networks," J. Non-Cryst. Solids 192&193 (1995) 79-91.
[18] L.W. Hobbs, C.E. Jesurum, B. Berger, Rigidity constraints in the amorphization of single- and multiply-polytopic structures, in: P.M. Duxbury, M.F. Thorpe (Eds.), Rigidity Theory and Applications, Plenum Press, New York, 1999, pp. 191–216. L. W. Hobbs, C. E. Jesurum, and B. Berger, "Rigidity constraints in amorphization of multiply-polytopic multiply-connected Ceramic Structures," in Microstructural Processes in Irradiated Materials (Symposium N), ed. S. J. Zinkle, G. Lucas, R. Ewing and J. Williams, Materials Research Society Symposium Proceedings 540 (1999) 717-728.
[19] P.K. Gupta, A.R. Cooper, Topologically disordered networks of rigid polytopes, J. Non-Cryst. Solids 123 (1–3) (1990) 14–21.
[20] L.W. Hobbs, C.E. Jesurum, V. Pulim, B. Berger, Local topology of silica networks, Philos. Mag. A 78 (3) (1998) 679–711.
[21] L.W. Hobbs, C.E. Jesurum, B. Berger, "The topology of silica networks," Ch. 1, in: J.P. Durand, R.A.B. Devine, E. Dooryee (Eds.), Structure and Imperfections in Amorphous and Crystalline Silica, John Wiley, London, 2000, pp. 1–47.
[22] L.W. Hobbs, Topology and geometry in the irradation-induced amorphization of insulators, Nucl. Instrum. Methods Phys. Res. B 91 (1–4) (1994) 30–42. L. W. Hobbs, "The role of topology and geometry in the irradiation-induced amorphization of network structures," J. Non-Cryst. Solids 182 [1-2] (1995) 27-39.
[23] M.F. Thorpe, D.J. Jacobs, N.V. Cubynsky, A.J. Rader, Generic rigidity of network glasses, in: P.M. Duxbury, M.F. Thorpe (Eds.), Rigidity Theory and Applications, Plenum Press, New York, 1999, pp. 239–277.
[24] J. Tersoff, Chemical order in amorphous silicon carbide, *Phys. Rev.* B 49 (23) (1994) 16349–16352.
[25] X. Yuan, L.W. Hobbs, Modeling chemical and topological disorder in irradiation-amorphized silicon carbide, *Nucl. Instrum. Methods Phys. Res.* B 191 (1–4) (2002) 74–82.
[26] X. Yuan, L.W. Hobbs, "Influence of interatomic potentials in MD investigation of ordering in a-SiC," in *microstructural Processes in irradiated materials* (symposium R), Mater. Res. Soc. Symp. Proc. 650 (2000) R13, 8 (1-6).
[27] J.P. Rino, I. Ebbsjö, P.S. Branicio, R.K. Kalia, A. Nakano, F. Shimojo, P. Vashishta, Short- and intermediate-range structural correlations in amorphous silicon carbide:A molecular dynamics study, Phys. Rev. B 70 (4) (2004) 045207 (1-11).
[28] A. Debelle, A. Boulle, A. Chartier, F. Gao, W.J. Weber, Interplay between atomic disorder, lattice swelling, and defect energy in ion-irradiation-induced amorphization of SiC, Phys. Rev. B 90 (2014) 174112.
[29] F. Gao, W.J. Weber, Cascade overlap and amorphization in (formula presented) Defect accumulation, topological features, and disordering, Phys. Rev. B Condens. Matter 66 (2002) 1–10.
[30] F. Finocchi, G. Galli, M. Parrinello, C.M. Bertoni, Microscopic struture of amorphous covalent alloys probed by *ab initio* molecular dynamics: SiC, Phys. Rev. Lett. 68 (20) (1992) 3044–3047.
[31] J. Li, Transformation strain by chemical disordering in silicon carbide, J. Appl. Phys. 95 (1) (2004) 6466–6469.
[32] C. Jiang, M.-J. Zheng, D. Morgan, I. Szlufarska, Amorphization driven by defect-induced mechanical instability, Phys. Rev. Lett. 111 (15) (2013) 155501, 1-5.
[33] D.K. Saldin, The theory of electron energy-loss near-edge structure, Philos. Mag. B Phys. Condens. Matter; Stat. Mech. Electron. Opt. Magn. Prop. 56 (1987) 515–525.
[34] D.R. McKenzie, S.D. Berger, L.M. Brown, Bonding in a-$Si_{1-x}C_x$: H films studied by electron energy loss near-edge structure, Solid State Commun. 59 (5) (1986) 325–329.
[35] S. Muto, T. Tanabe, T. Shibayama, H. Takahashi, Damaging process of α-SiC under electron irradiation studied with electron microscopy and spectroscopy, Nucl. Instrum. Methods Phys. Res. B 191 (1–4) (2002) 519–523.
[36] S. Muto, T. Tanabe, Local structures and damage processes of electron irradiated α-SiC studied with transmission electron microscopy and electron energy-loss spectroscopy, J. Appl. Phys. 93 (7) (2003) 3765–3775.
[37] N. Asaoka, S. Muto, T. Tanabe, "Formation of Si clusters in electron-irradiated SiC studied by electron energy-loss spectroscopy," *Diamond Relat*, Materials 10 (3–7) (2001) 1251–1254.
[38] A. Chehaidar, R. Carles, A. Zwick, C. Meunier, B. Cros, J. Durand, Chemical bonding analysis of a-SiC H films by Raman spectroscopy, J. Non-Cryst. Solids 169 (1–2) (1993) 37–46.
[39] W. Bolse, Amorphization and recrystallization of covalent tetrahedral networks, Nucl. Instrum. Methods Phys. Res. B 148 (1–4) (1999) 83–92.
[40] N. Chaâbane, A. Debelle, G. Sattonnay, P. Trocellier, Y. Serruys, L. Thomé, Y. Zhang, W.J. Weber, C. Meis, L. Gosmain, A. Boulle, Investigation of irradiation effects induced by self-ion in 6H-SiC combining RBS/C, Raman and XRD, Nucl. Instrum. Methods Phys. Res. B 286 (2012) 108–113.
[41] M. Gorman, S.A. Solin, Direct evidence for homonuclear bonds in amorphous SiC, Solid State Commun. 15 (4) (1974) 761–765.
[42] P.F. Wang, L. Huang, W. Zhu, Y.F. Ruan, Raman scattering of neutron irradiated 6H-SiC, Solid State Commun. 152 (10) (2012) 887–890.
[43] P.F. Wang, Y.F. Ruan, L. Huang, W. Zhu, Nitrogen-promoted formation of graphite-like aggregations in SiC during neutron irradiation, J. Appl. Phys. 111 (6) (2012) 063517 (1-4).
[44] P. Wang, Y. Chen, W. Zhu, L. Huang, J. Chen, B. Hou, Y. Ruan, "Analysis of correlation between irradiation produced C clusters and intentionally incorporated N impurity in SiC, Diam. Relat. Mater. 29 (2012) 48–51.
[45] H. Inui, H. Mori, A. Suzuki, H. Fujita, Electron-irradiation-induced crystalline-to-amorphous transition in β-SiC single crystals, Philos. Mag. A B 65 (1) (1992) 1–14.
[46] A.E. Kaloyeros, R.B. Rizk, J.B. Woodhouse, Extended x-ray-absorption and electron-energy-loss fine-structure studies of the local atomic structure of amorphous unhydrogenated and hydrogenated silicon carbide, Phys. Rev. B 38 (18) (1988) 13099–13106.
[47] M. Ishimaru, I.-T. Bae, Y. Hirotsu, S. Matsumura, K.E. Sickafus, Structural relaxation of amorphous silicon carbide, Phys. Rev. Lett. 89 (2002) 055502.
[48] M. Ishimaru, A. Hirata, M. Naito, I.T. Bae, Y. Zhang, W.J. Weber, Direct observations of thermally induced structural changes in amorphous silicon carbide,

J. Appl. Phys. 104 (2008).
[49] W. Bolse, Amorphization and recrystallization of covalent tetrahedral networks, Nucl. Instrum. Methods Phys. Res. Sect. B Beam Interact. Mater. Atoms 148 (1999) 83–92.
[50] G. Kresse, J. Furthmüller, Efficient iterative schemes for *ab initio* total-energy calculations using a plane-wave basis set, Phys. Rev. B 54 (16) (1996) 11169–11186.
[51] J.P. Perdew, K. Burke, M. Ernzerhof, Generalized gradient approximation made simple, Phys. Rev. Lett. 77 (18) (1996) 3865–3868.
[52] G. Kresse, D. Joubert, From ultrasoft pseudopotentials to the projector augmented-wave method, Phys. Rev. B 59 (3) (1999) 1758–1775.
[53] H.J. Monkhorst, J.D. Pack, Special points for Brillouin-zone integrations, Phys. Rev. B 13 (12) (1976) 5188–5192.
[54] W.G. Hoover, Canonical dynamics: equilibrium phase-space distributions, Phys. Rev. 31 (3) (1985) 1695–1697.
[55] The FEFF Project, Department of Physics, University of Washington, Seattle, WA, 2017. http://leonardo.phys.washington.edu/feffproject-feff.html. (Accessed February 2017).
[56] M.S. Moreno, K. Jorissen, J.J. Rehr, Practical aspects of electron energy-loss spectroscopy (EELS) calculations using FEFF8, Micron 38 (1) (2007) 1–11.
[57] J.J. Rehr, J.J. Kas, F.D. Vila, M.P. Prange, K. Jorissen, Parameter-free calculations of X-ray spectra with FEFF9, Phys. Chem. Chem. Phys. 12 (21) (2010) 5503–5513.
[58] K. Jorissen, J. Rehr, J. Verbeeck, Multiple scattering calculations of relativistic electron energy loss spectra, *Phys. Rev.* B 81 (15) (2010), 155108-(1-6).
[59] Yi Zhang, Computer Simulation and Topological Modleing of Radiation Effects in Zircon, Ph.D. thesis, MIT, Cambridge, MA, 2006. Leslie Dewan, "Molecular dynamics simulation and topological analysis of the network structure of actinide-bearing materials," Ph.D. thesis (MIT, Cambridge, MA, 2013.
[60] H.R. Foxhall, K.P. Travis, L.W. Hobbs, S.C. Rich, S.L. Owens, Understanding the radiation-induced amorphization of zirconolite using molecular dynamics and conectivity topology analysis, Phil. Mag. B 93 (4) (2013) 328–355.
[61] M. Micoulaut, X. Yuan, L.W. Hobbs, Coordination and intermediate-range order alterations in densified germania, J. Non-Cryst. Solids 353 (18-21) (2007) 1963–1965.
[62] M. Ishimaru, Electron-beam radial distribution analysis of irradiation-induced amorphous SiC, Nucl. Instrum. Methods Phys. Res. B 250 (1–2) (2006) 309–314.
[63] F. Finocchi, G. Galli, M. Parrinello, C.M. Bertoni, Structural properties of amorphous SiC via *ab-initio* molecular dynamics, J. Non-Cryst. Solids 137–138 (Part 1) (1991) 153–156.
[64] F. Finocchi, G. Galli, M. Parrinello, C.M. Bertoni, Microscopic struture of amorphous covalent alloys probed by *ab initio* molecular dynamics: SiC, Phys. Rev. Lett. 68 (20) (1992) 3044–3047.
[65] L.W. Hobbs, X. Yuan, Topology and topological disorder in silicas, in: G. Pacchioni, L. Skuja, D. Griscom (Eds.), Defects in SiO_2 and Related Dielectrics: Science and Technology, Kluwer, Dordrecht, Netherlands, 2000, pp. 37–41.